Journal Européen des Systèmes Automatisés
Vol. 59, No. 1, January, 2026, pp. 113-124
Journal homepage: http://iieta.org/journals/jesa

Application of the Rao-1 Algorithm for Maximum Power Point Tracking in PV Systems: Analysis and Implementation

Zouaoui Berrabah[1*], Mohamed Khadraoui[1], Mimoun Younes[2]

[1] Laboratory of Elaboration and Characterization of Materials (LECM), Electronics Department, Faculty of Electrical Engineering, Djilali Liabès University of Sidi Bel Abbès, Sidi Bel Abbès 22000, Algeria
[2] Laboratory of Elaboration and Characterization of Materials (LECM), Department of Mechanics, Faculty of Technology, Djilali Liabès University of Sidi Bel Abbès, Sidi Bel Abbès 22000, Algeria

Corresponding Author Email: zouaoui.berrabah@univ-sba.dz

https://doi.org/10.18280/jesa.590111

Received: 27 November 2025
Revised: 18 January 2026
Accepted: 26 January 2026
Available online: 31 January 2026

Keywords:
metaheuristic optimization, Maximum Power Point, MATLAB/Simulink, PV systems, Rao-1 algorithm, Particle Swarm Optimization, Perturb and Observe

ABSTRACT

An analysis of the Rao-1 metaheuristic optimization algorithm is conducted to evaluate its effectiveness for tracking Maximum Power Point (MPPT) in solar energy systems. The primary aim of this work is to enhance energy conversion efficiency under fluctuating environmental conditions, including variations in solar irradiance and ambient temperature. Rao-1, known for its parameter-less structure and low computational complexity, is implemented as an MPPT controller and benchmarked against two widely used methods: Perturb and Observe (P&O) and Particle Swarm Optimization (PSO). The device, including the ISOPHOTON IS_75/12 module and a DC–DC boost converter, is implemented in MATLAB/Simulink. All algorithms are evaluated using standardized test conditions that replicate real-world operating scenarios. Performance is assessed based on tracking efficiency, convergence speed, dynamic response, stability, and robustness to environmental variability. Simulation results demonstrate that the Rao-1 algorithm reliably surpasses both P&O and PSO for all metrics. Notably, Rao-1 achieves the optimal power point with reduced convergence time significantly reduces steady-state oscillatory behavior and power dissipation, and delivers higher energy yield over time. Its ability to sustain accurate and stable tracking under fluctuating conditions underscores its robustness and potential for practical deployment in advanced PV energy systems.

1. INTRODUCTION

Electricity is essential for modern life, driving economic growth and technological advancement. Rising global demand has highlighted the limitations of fossil fuels, leading to higher energy costs and increased greenhouse gas emissions [1].

In response to these challenges, the scientific community has intensified efforts to identify viable alternatives to fossil fuels. Solar energy is acknowledged as one of the most important sustainable energy sources. Unlike finite fossil fuels, solar energy is inexhaustible, widely available, and environmentally sustainable. In addition to being a non-polluting alternative to traditional fuels, it provides widespread access to electricity, particularly in remote or off-grid regions, without requiring extensive transmission infrastructure for applications like lighting or irrigation [2].

Despite the promise of solar energy, its large-scale adoption is hindered by the relatively low efficiency of solar cells, which currently does not exceed 24%, which varies with cell type and radiation intensity [3, 4]. Additionally, PV systems have nonlinear current-voltage (I-V) and power-voltage (P-V) characteristics, having a key operating point called the Maximum Power Point (MPPT). Operating at the MPPT ensures that the system delivers its highest possible power output [5, 6]. However, fluctuating factors such as the angle of solar incidence, ambient temperature, and irradiance intensity, affected by daily and seasonal solar movement or shading from weather conditions, can cause the system to deviate from this optimal point.

To overcome these limitations and improve the efficiency of energy conversion, Recent research has increasingly concentrated on advanced control strategies for PV applications, particularly MPPT techniques. In this context, metaheuristic optimization–based MPPT algorithms have obtained notable attention due to their strong global search capability, rapid convergence, and robustness under nonlinear and time-varying operating conditions. Representative examples include the Jaya algorithm, which directs solutions toward the optimal by avoiding the worst [7]; Gorilla Troops Optimizer (GTO), inspired by social behaviors [8]; and the Runge–Kutta Optimizer, which utilizes numerical integration for solution updates [9]. These approaches have been widely applied to MPPT problems in PV systems owing to their robustness and fast convergence. Within this class of methods, the Rao-1 algorithm is defined by its simple yet effective optimization framework that does not require algorithm-specific control parameters, making it well suited for real-time execution. When applied to MPPT control [10]. By

continuously estimating the MPPT in real time, such algorithms ensure optimal PV system operation, thereby maximizing power extraction and enhancing overall system efficiency [11].

2. PROPOSED SYSTEM

The studied PV system comprises a PV panel and a load connected via a boost DC–DC converter. The DC output voltage is stabilized by the boost converter, which is powered by the PV generator, making it suitable for applications such as battery charging or subsequent DC–AC conversion. Its primary work is to use controlled voltage regulation to maximize the power extraction of the PV generator. To perform this operation, the MPPT controller continuously adjusts the converter's duty cycle based on real-time measurements of the PV generator's power, voltage, or current. The running at the optimum power point realized by the controller improves the efficiency of energy transfer and the overall performance of the energy system [12]. A schematic presentation of this system is depicted in Figure 1.

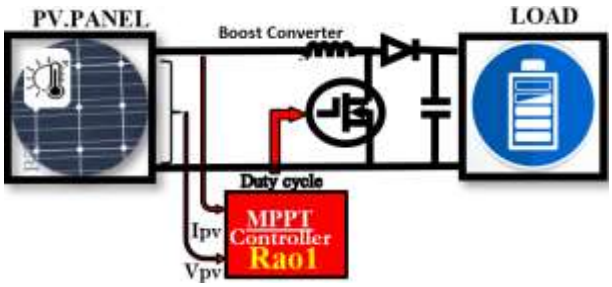

Figure 1. Block diagram of the proposed system

2.1 Solar panel models

PV modeling uses mathematical formulas to forecast how well solar panels will function electrically in a variety of environmental circumstances, including temperature, shade, and irradiance. The models characterize both individual solar cell behavior and the aggregate performance of PV modules. Key parameters, including cell efficiency, series and shunt resistances, and shading losses, are considered to accurately represent real operating conditions. Such modeling is vital for performance analysis and optimization, enabling improved design, control, and energy conversion efficiency of PV systems [13].

2.1.1 Modelling of the ideal and practical PV cell

A solar cell, or PV cell, is a semiconductor device that converts incident sunlight to electrical energy through the PV effect, forming the basic unit of PV modules used in renewable energy systems. The device consists of a thin semiconductor structure with a p–n junction, where the electrical response, including voltage and current, depends on illumination. Solar cells function under both artificial and natural light sources and are the basic components of PV modules, or solar panels [14].

In the absence of illumination, the I–V characteristic of a solar cell exhibits exponential behavior similar to that seen in a diode. Electron-hole pairs are created when photons with energy higher than the semiconductor bandgap are absorbed. The internal electric field of the p–n junction then separates these charge carriers, resulting in a current proportional to the incident radiation. This current passes through the circuit outside in the case of a circuit that is shorted. However, the inherent p-n junction diode shunts it internally when it is in an open-circuit state. As a result, this diode's properties control the solar cell's open-circuit voltage performance [15]. A PV cell is frequently represented in the literature as a current source linked in parallel with the diode that represents the p-n junction. Shockley's traditional single-diode model, which can be applied to PV modules by joining identical cells in parallel or series, captures this behavior [16].

The ideal solar cell's I-V characteristic is defined by Eq. (1).

$$I_{cell}=I_{ph}-I_0\left[\exp\left(\frac{q\,V_{cell}}{n\,k\,T}\right)-1\right] \quad (1)$$

I_{cell} and V_{cell} correspond to the PV cell's electrical output. The term I_{ph} refers to the photocurrent induced by incident solar radiation [A], and it increases with both solar irradiation and temperature. I_0 is the diode leakage current, whose magnitude is influenced by temperature variations. Where n is the diode ideality factor reflecting semiconductor quality and typically ranging from 1 to 2. The constant q represents the electron charge ($1.60217646 \times 10^{-19}$ C), while k denotes the Boltzmann constant ($1.3806503 \times 10^{-23}$ J/K), and T indicate the p–n junction temperature [K]. The PV cell output current results from the difference between the generated photocurrent and the diode current. To accurately model practical I–V characteristics, the shunt resistance and series resistance are included [17].

The shunt resistance Rsh models surface leakage currents caused by junction non-idealities and impurities, while the series resistance Rs represents internal losses from contact and semiconductor resistances. Despite adding complexity, including Rs in PV modeling greatly improves engineering accuracy and practicality [18]. The ideal and practical circuit representations of the PV cell are presented in Figure 2.

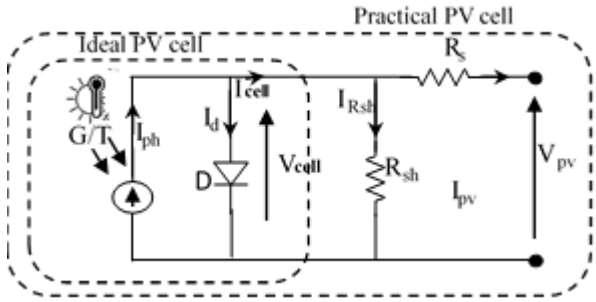

Figure 2. Ideal and practical PV cell circuit model

The output current I_{pv} of this model is the current supplied by the PV cell [A]. It can be calculated utilizing Kirchhoff's law, which is represented as: $I_{pv} = I_{ph} - I_d - I_{sh}$. Here, I_{ph} stands for photocurrent, Id for diode current, and Ish for shunt current.

The modeling of solar cells' real I-V characteristics for practical engineering analysis is shown in Eq. (2).

$$I_{pv}=I_{ph}-\underbrace{I_0\left[\exp\left(\frac{q\left(V_{pv}+R_s I_{pv}\right)}{n\,k\,T}\right)-1\right]}_{I_d}-\underbrace{\frac{V_{pv}+R_s I_{pv}}{R_{sh}}}_{I_{sh}} \quad (2)$$

where, R_s stands for the series resistance. [Ω] and R_{sh} refers

to the parallel (or shunt) resistance [Ω].

The photo-current of the PV cell is according to Eq. (3).

$$I_{ph}=\underbrace{[I_{sc.ref}+K_i(T-T_{ref})]}_{I_{sc}}\frac{G}{G_{ref}} \quad (3)$$

where, I_{sc} stands for current in a short circuit ($I_{ph} = I_{sc.ref}$: light-generated current at reference conditions: 25℃ / 1000 W/m^2) [A]. Ki is the temperature coefficient of short-circuit current provided by the manufacturer. T is the cell temperatures at outdoor conditions [Kelvin]. T_{ref} is the cell's reference temperature. [25 + 273 = 298 Kelvin]. G_{ref} stands for reference irradiation. [1000 w/m²]. G is the surface irradiance of the cell [w/m²].

An ordinary PV cell provides just over 2 watts of power at around 0.5 volts, so to generate higher power, these cells need to be linked together in a series-parallel to form a solar panel [19].

The Shockley diode equation of the practical PV cell may be expressed by Eq. (4).

$$I_d=I_0\left[\exp\left(\frac{q(V_{pv}+R_sI_{pv})}{N_s\,n\,k\,T}\right)-1\right] \quad (4)$$

N_s is the total number of solar cells in the PV panel that are electrically connected in series (given by the manufacturer).

The reverse saturation current of the diode, I_0 may be expressed by Eq. (5).

$$I_0=I_{0.ref}\left(\frac{T}{T_{ref}}\right)^3\exp\left[\frac{qE_g}{n\,k}\left(\frac{1}{T_{ref}}\right)-\left(\frac{1}{T}\right)\right] \quad (5)$$

where, E_g denotes the cell's semiconductor's bandgap energy. (For the polycrystalline Si at 25 C, $E_g \approx 1.12$ eV).

$I_{0.ref}$ is the reference reverse saturation current, which is described as Eq. (6).

$$I_{0.ref}=I_{sc}/\left[\exp\left(\frac{qV_{oc}}{N_s\,n\,k\,T}\right)-1\right] \quad (6)$$

where, I_{sc} is the short circuit current, and V_{oc}, represent solar cell's open circuit voltage [$V_{oc} = V_{oc.ref} + Kv\ (T-Tr)$], and Kv is the V_{oc} temp. coefficient. Generally, such values can be found in PV module datasheets.

I_{sh} is the current through the shunt resistor, which is described as Eq. (7).

$$I_{sh}=\frac{V_{pv}+R_sI_{pv}}{R_{sh}} \quad (7)$$

2.1.2 PV module and array modeling

In commercial PV goods, PV cells are generally connected in series to constitute a PV module, guaranteeing a high enough operating voltage. Eq. (8) represents the modeling of the practical PV panel's I-V characteristic.

$$I_{pv}=I_{ph}-I_0\left[\exp\left(\frac{q(V_{pv}+R_sI_{pv})}{N_s\,n\,k\,T}\right)-1\right]-\frac{V_{pv}+R_sI_{pv}}{R_{sh}} \quad (8)$$

2.1.3 Detailed modeling

The ISOPHOTON IS-75/12 PV module is used as the reference model for simulation. It is modeled in MATLAB/Simulink, and its detailed electrical specifications are offered in Table 1.

Table 1. Typical electrical characteristic of ISOPHOTON IS-75/12

Maximum Power (Pmpp)	Max. Power Point Voltage (Vmpp)	Max. Power Point Current (Impp)	Open Circuit Voltage (Voc)	Short-Circuit Current (Isc)	Parallel Connected Strings (Np)
75.1 W	17.3 V	4.34 A	21.6 V	4.67 A	1

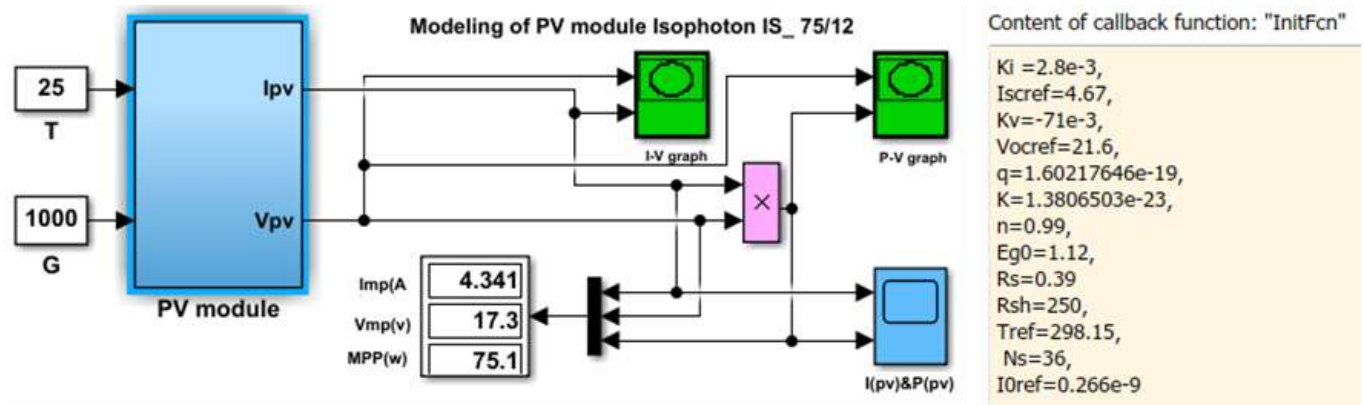

Figure 3. Simulink implementation of the ISOPHOTON IS-75/12 PV module

Block diagram of ISOPHOTON IS-75/12 PV module modeled in MATLAB Simulink is shown in Figure 3.

The I-V and P-V characteristics of the ISOPHOTON IS-75/12 Panel under standard test conditions (STC:1000 W/m², 25℃,) are displayed in Figure 4.

The Simulink implementation representative of Eq. (2) using Kirchhoff's law.is shown in Figure 5.

Figure 6 demonstrates Eq. (3) used to compute photocurrent based on irradiance and temperature.

Figure 7 represents the diode current calculated using the Shockley Eq. (4).

The Simulink implementation is representative of Eq. (5) using Kirchhoff's law.is apparent in Figure 8.

Figure 9 shows the calculation of reference saturation current based on the voltage at the open circuit and the current at the short circuit, which represents Eq. (6).

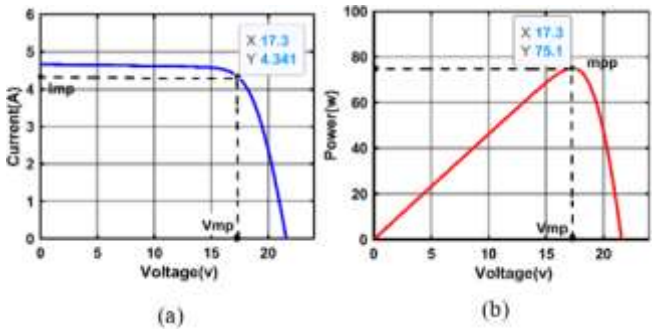

Figure 4. PV module characteristics at STC: (a) I-V curves (b) P-V curves

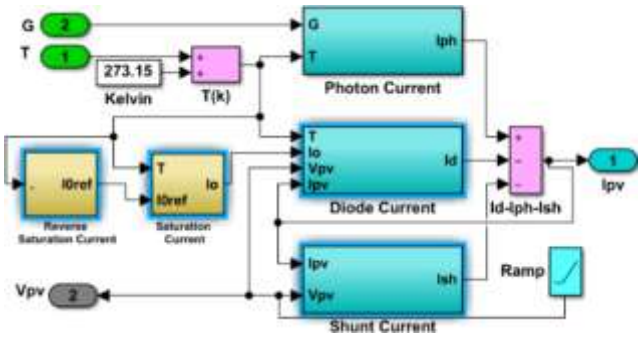

Figure 5. Detailed implementation of the Ipv

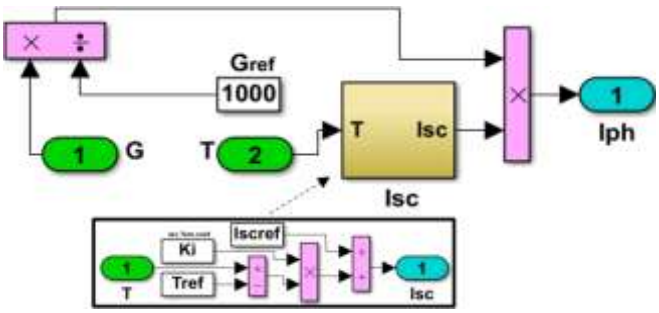

Figure 6. Detailed implementation of the Iph

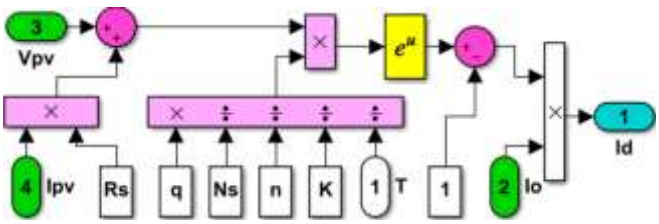

Figure 7. Detailed implementation of the diode current Id

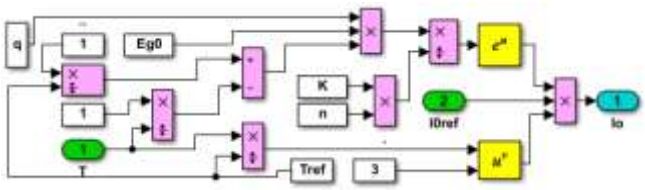

Figure 8. Detailed implementation of the diode current Io

The current Ish is represented by the Simulink implementation representative of Eq. (7) in Figure 10.

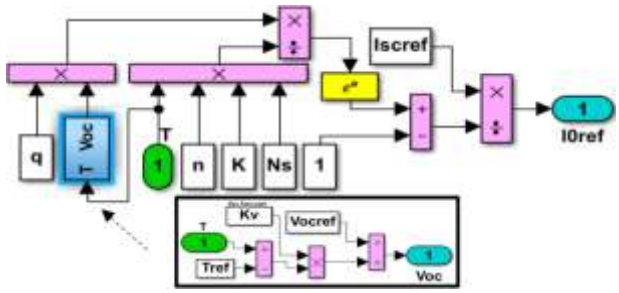

Figure 9. Simulink implementation of I0.ref

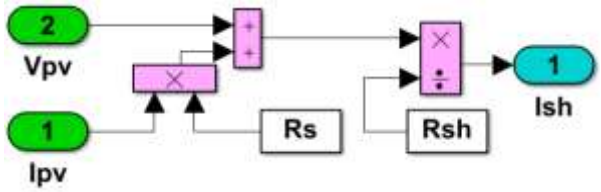

Figure 10. Detailed implementation of Ish

2.1.4 Impact of temperature variations on the solar panel's I-V and P-V characteristics

Temperature-induced changes in the I–V and P–V curves are evident when modifying the temperature between 15°C and 65°C, and irradiance is fixed at 1000 W/m². Rising temperature adversely affects the PV module by reducing the open-circuit voltage, which in turn decreases the delivered power, as shown in Figure 11.

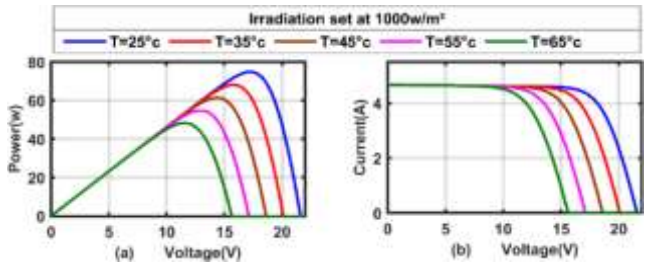

Figure 11. Impact of varying temperature at consistent irradiance: (a) P-V curves (b) I-V curves

2.1.5 Impact of irradiance variations on the solar panel's I-V and P-V characteristics

The change in insolation intensity has a noticeable effect on the I-V and P-V graphs by modifying a solar radiation from 300 watts/m² to 1000 watts/m², and the temperature is fixed at 25°C. As solar radiation increases, the PV module is able to generate more power because of the noticeable rise in current. This rise in current causes higher peak levels in the P-V and I-V contours, as seen in Figure 12.

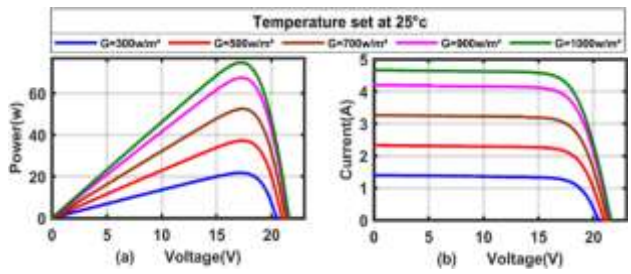

Figure 12. Impact of varying insolation at consistent temperature: (a) P-V curves (b) I-V curves

2.1.6 Impact of varying temperature and insolation on the solar panel's I-V and P-V characteristics

Figure 13 shows the I-V and P-V characteristic curves for different levels of sunlight and temperatures. It was found that at the rise of the temperature, the PV module's output voltage decreases linearly, but the current remains relatively stable. This drop in voltage results in a reduction of the PV module's power output, where the sunlight level stays unchanged. Additionally, although temperature possesses a minor influence on the shorter circuit current, this effect becomes more significant as the amount of sunlight increases.

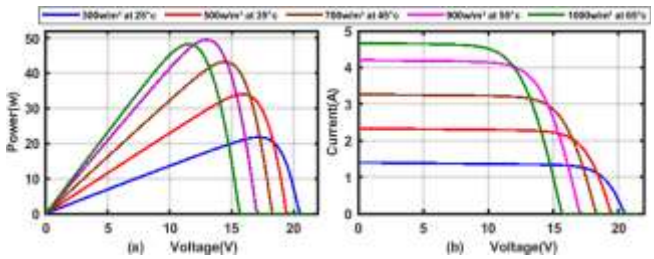

Figure 13. Impact of varying temperature and insolation: (a) P-V curves (b) I-V curves

2.2 DC-DC boost converter

One of the primary issues with PV systems is that variations in insolation and temperature possess an impact upon the resultant voltage of PV panels. As a result, loads cannot be directly linked to the PV panels' output. Because of this, a DC-DC converter was connected between them; it must function as an interface between these two stages in order to match impedance by altering the switch's duty cycle (D) [20]. The core of MPPT hardware is this converter. It is an electrical circuit that changes the voltage level of a direct current (DC) source. For chopper converters, there are numerous topologies. One of these topologies is a boost converter, which raises the voltage to keep the PV generator's maximum output voltage constant under all circumstances. It is composed of two capacitors (C1 and C2), an inductor (L), a MOSFET acting as a switch (S), a diode (D), a resistor acting as a load, and an input voltage source (Vin = Vpv). The role of input capacitor C1 is to smooth the input voltage and provide a low-impedance current source to the switch. This helps reduce input voltage ripple and output power fluctuations of the PV array, thereby improving converter efficiency. While the role of the output capacitor C2 is to store energy and supply it to the load when the switch is off. This helps stabilize the output voltage level by reducing ripple [21]. The structure of the boost converter is depicted in Figure 14.

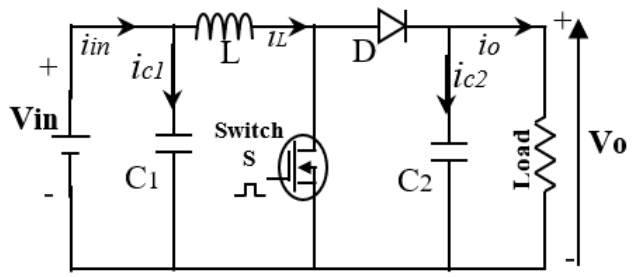

Figure 14. The boost converter's circuit schematic

The boost converter specifications chosen in this research are shown in Table 2.

Table 2. Specific DC–DC boost converter electrical variables

Variables	Values	
Input capacitor C1	6e-6	F
Inductance L	2e-4	H
Output capacitor C2	9e-6	F
Resistor	3.986	Ω
Frequency	20,000	Hz

2.3 Implementation of the Maximum Power Point method

The purpose of the MPPT is to maintain that a PV panel operates continuously at its MPPT in spite of variations in atmospheric conditions such as temperature and solar irradiance. The electrical power generated by a PV panel is strongly dependent on these environmental factors. For each specific combination of irradiance and temperature, there exists a unique MPPT that's where the PV cells deliver their maximum available power. By operating the solar panels at this stage, energy extraction is maximized and the system's overall efficiency is greatly increased [22].

2.3.1 Perturb and observe technique

The primarily popular method for determining the MPPT in solar systems is the perturb and observe strategy. Its popularity is a result of how easy it is to deploy and how only the voltage and current of the solar generator need to be measured. The idea behind this technique is to continuously disrupt the voltage by raising or lowering it., after which the resulting power is observed [23] The process goes as follows: the algorithm causes a disturbance with a slight increase in voltage adjusting to the duty cycle, i.e., the difference between the new and the prior voltage is positive ($dv > 0$), then we notice that the fresh power is bigger than the prior one ($dp > 0$); at this moment, the functioning point becomes on the left; it is in the right direction, approaching the MPPT; therefore, the disturbance must continue at this slight increase in voltage. If it is the reverse and the new power is lower than the previous one ($dp < 0$), then here the working point is located on the right in the wrong direction, far from the point of maximum power, here the disturbance process must be reversed, so the duty cycle must make a slight decrease in voltage, which means the difference between the new and the previous voltage is negative ($dv < 0$) Then it notes again, if the fresh power is bigger than the prior one ($dp > 0$), the process continues the disturbance by decreasing the voltage because the working point is now located on the right. direction by approaching the maximum power, then the logarithm repeats the observation again, and if it finds that the new power has started to decrease compared to the old one ($dp < 0$), and the operating point has again moved to the left and has started to move away in the wrong direction, the disturbance reverses until the operational point's trajectory returns to the optimal power orientation [24].

The principle of this process is shown in Figure 15. The Perturb and Observe (P&O) algorithm repetitively oscillates around the MPPT, but its effectiveness and precision may not match other more intricate MPPT algorithms, especially when faced with certain circumstances. Instances such as sudden changes in panel temperature or partial shading can pose challenges for P&O. Despite being a low-cost and straightforward algorithm, it may not always be the most optimal choice [25]. This method's structure is described in Figure 16.

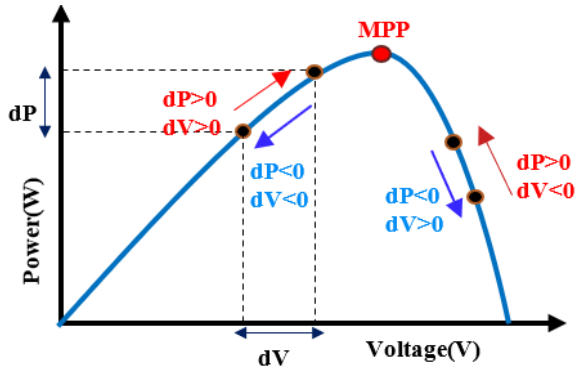

Figure 15. Perturb and Observe (P&O) algorithm operating principle

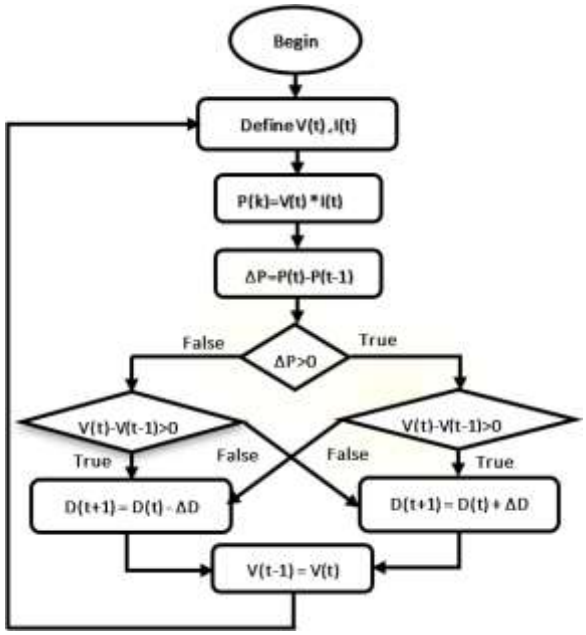

Figure 16. Flowchart for the Perturb and Observe (P&O) Maximum Power Point (MPPT) strategy

2.3.2 Particle Swarm Optimization

It is a clever design technique and robust metaheuristic algorithm inspired by the social behavior of animals, particularly birds. Kennedy and Eberhart first presented it in 1995 as a method for resolving optimization issues in ongoing search spaces [26].

It has perks such as simple execution, rapid convergence, and the capacity to efficiently reach the global optimum, even in complex, nonlinear, discontinuous, and non-differentiable curves. In an n-dimensional space, several particles are employed. A population of arbitrary solutions is used to initialize the framework. A random velocity is also assigned to each possible answer; these solutions are referred to as particles [27].

The fundamental idea behind the Particle Swarm Optimization (PSO) is to use a group of particles' collective social behavior to investigate and identify the best solution. Every particle inside the group is impacted by the other particles' present positions as well as its optimal position. While each particle's Pbest represents the best solution it found independently, the Gbest indicates the best solution discovered by a unique element of the group. To discover an ideal response to the challenge, any particle contains a function which must be optimized by a determined adaptation value (fitness value) and the velocity vector, which can determine its search direction and distance, which help all particles navigate towards both the best global position and their individual best positions [28].

The procedure of adjusting the position and velocity of the particles is shown graphically in Figure 17.

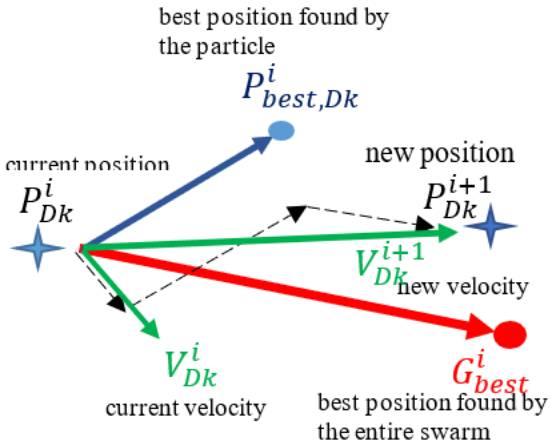

Figure 17. Particle Swarm Optimization (PSO) particle motion illustration

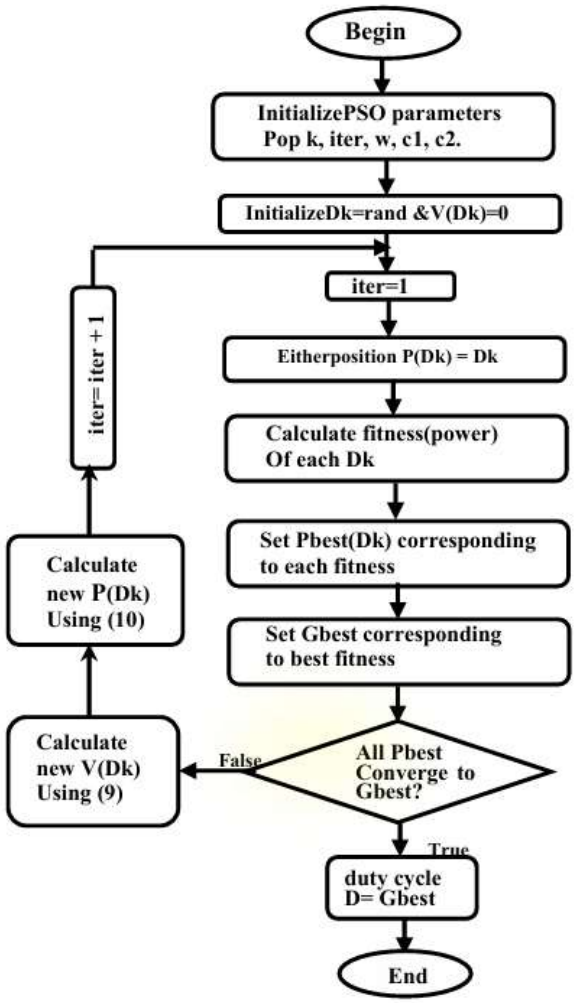

Figure 18. Flowchart of the Particle Swarm Optimization (PSO) Maximum Power Point (MPPT) algorithm

The duty cycles Dk of the boost converter serve as particles

in this application, functioning as optimization variables. k = (1, 2, ... m), m represents the quantity of particles. Maximizing the intended function (power), which is the result of multiplying the output voltage by the current, is the main target. Therefore, finding and identifying the MPP is the goal of the PSO method. In the initial iteration, particles are assigned random values as their initial positions and zero values as their initial velocities. The principle of this technique is established for each variable to identify its individual best position (Pbest), while the general best position (Gbest) is determined by the best objective function [29]. If convergence does not occur, the algorithm calculates the new velocity (Vnew.k) and the new position (Pnew.k) using Eqs. (9) and (10) and proceeds to the next iteration. The new position for each particle allows the calculation of the improved objective function, Pbest values, and the improved Gbest value. The process continues until convergence is achieved for all Pbest, reaching the final Gbest value, which has to do with the most recent enhanced duty cycle. This indicates that the MPP has been reached. and the PSO algorithm concludes its operation [30]. These phases are represented by the flowchart in Figure 18.

The updated velocity V_{Dk}^{i+1} of the particle is determined by considering its previous velocity, adding the variance between its present position and its optimal position, and the disparity between the global optimum and the particle's current whereabouts [31], which is shown in Eq. (9), and the updated position P_{Dk}^{i+1} of the particle Dk is given by Eq. (10).

$$V_{Dk}^{i+1}=W*V_{Dk}^{i}+c1*r1*\left(P_{best,Dk}^{i}-P_{Dk}^{i}\right)+c2*r2*(G_{best}^{i}-P_{Dk}^{i}) \quad (9)$$

$$P_{Dk}^{i+1}=P_{Dk}^{i}+V_{Dk}^{i+1} \quad (10)$$

where, P_{Dk}^{i} and V_{Dk}^{i} it refers to the prior position and velocity of the particle D_k during iteration i, ω denotes the inertia weight, c1 and c2 serve as the accelerating coefficients, r1 and r2 are arbitrary variables evenly spread in [0,1].

2.3.3 Rao-1 metaheuristic algorithm

Ravipudi Venkata Rao developed the Rao-1 algorithm in 2019. It is one of the three variants in the Rao group, which include Rao-2 and Rao-3. It is a metaphor-free optimization method. Rao-1 is recognized for its computational efficiency and is well suited for continuous nonlinear optimization problems, both constrained and unconstrained. Its procedure consists of initializing a population of candidate solutions, applying evolutionary update rules, and selecting improved solutions according to the Rao optimization framework The Rao-1 algorithm became famous for its simple design and quick convergence towards the optimal solution. In order to increase performance, it integrates random interactivity among candidate solutions using the finest and worst solutions discovered during the search process. Furthermore, it eliminates the need for complicated parameter adjustment by requiring only a few fundamental control factors, such as population size and iteration count. These characteristics make Rao-1 a powerful and practical method for overcoming a diverse range of optimization issues [32].

Assuming there is a component 'm' (j = 1, 2, ..., m) and 'n' candidate solutions (k = 1, 2, ..., n), allow f(x) refer to the desired function that the optimization process aims to be maximize or minimize. In each iteration, the finest candidate represents the ideal f(x) value (f(x)best), whereas the poorest candidate represents the lowest f(x) value (f(x)worst) among all candidates of the set. If Z (j,k,i) defines the value of the jth variable for the kth candidate throughout the ith iteration, updated according to Eq. (11).

$$Z_{j,k,i}^{'}=Z_{j,k,i}+r_{1,j,i}(Z_{j,best,i}-Z_{j,worst,i}) \quad (11)$$

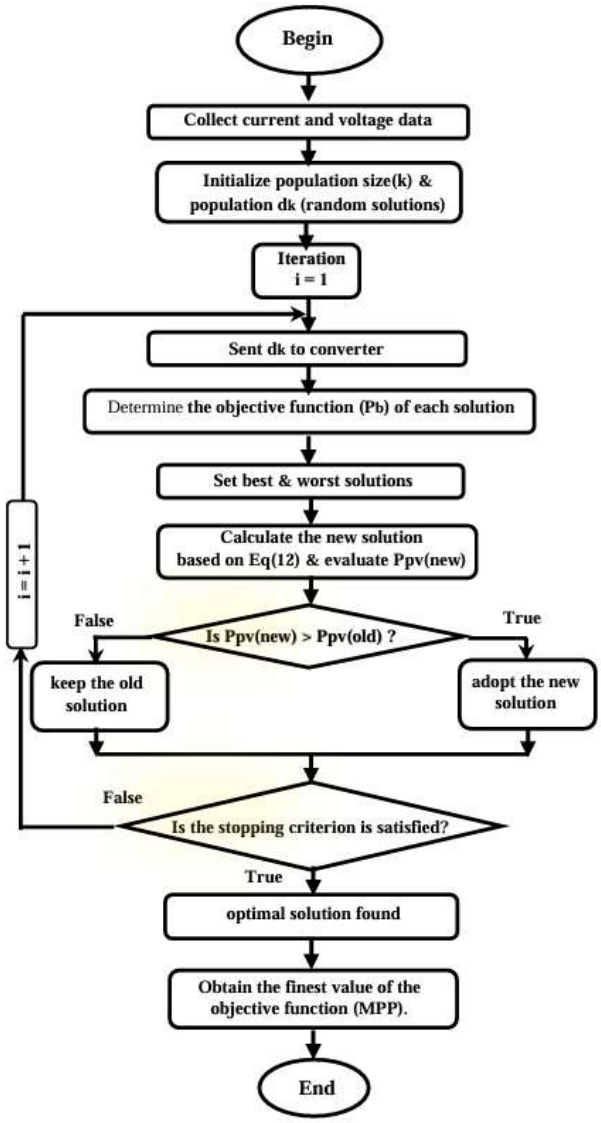

Figure 19. The flowchart of Rao-1 based Maximum Power Point (MPPT) control algorithm

2.3.4 Rao-1 based Maximum Power Point

In our research, the objective function f(x) is defined as the output power of the boost converter generated by the solar panel and is maximized. The decision variable refers to the duty cycle, which constitutes the candidate solution and is represented as a single design variable (i.e., j = m = 1), hence, the number of candidate solutions k (the population dimension) could change as k = 1, 2, ... 50. Accordingly, the best candidate is defined as the value of the duty cycle corresponding to the maximum value of the objective function f(x), whereas the lowest candidate is the value of the duty cycle associated with the minimum value of f(x) among all candidate solutions. The basic iterative formula of Rao-1 is described in the following Eq. (12).

$$d_{k,i}^{new}=D_{k,i}^{old}+r_i(d_{best,i}-d_{worst,i}) \quad (12)$$

where, $d_{k,i}^{new}$ is the updated value of $d_{k,i}^{old}$ which in turn represents the value of the previous duty cycle during the i^{th} iteration, and r denotes a uniformly distributed random variable over [0, 1].

The algorithm follows a basic iterative optimization process. Let's break down the steps of each iteration (i):

• First Step: Fill out the first table

Randomly assign candidate solutions.

For every solution, find the objective function (power of energy).

Determine which of the solutions have the best and worst values.

• Second Step: Fill out the second table

New candidate solutions are computed using the expression given in Eq. (12).

Evaluate the corresponding objective functions for the new solutions.

• Third Step: Fill out the third table

Comparison between the results of two candidate solutions of the same rank k from the first and second tables in terms of the best result.

Fill out the third table by listing only each good result and the corresponding candidate solution for each arrangement K.

Identify the best and worst values among the solutions.

At this point, the first iteration is complete. The algorithm then checks the termination criterion to determine whether the optimization process should be halted or not. If the termination criteria, which is achieving maximum power, is met, the algorithm will terminate. However, if the criterion is not met, the algorithm proceeds to the next iteration.

The algorithm begins by transferring all data and results from the third table of the previous iteration into the first table for the current iteration. This initiates the process, allowing it to proceed with the same steps as before: calculating new candidate solutions, evaluating the objective function, comparing the results, and updating the best solution [28]. These iterations continue until the algorithm reaches the perfect result. The optimization process of the Rao-1 algorithm is clearly illustrated in Figure 19.

3. SIMULATION RESULTS AND DISCUSSION

This study maximizes the power extracted from a PV panel by using a boost converter to implement the Rao-1, PSO, and P&O MPPT techniques. Their performances are evaluated under static meteorological conditions (1000 W/m² at 25°C) as well as under dynamic meteorological conditions (1000, 900, 700 and 1000 W/m² at temperatures of 25°C, 15°C, 20°C and 25°C, respectively).

3.1 Static meteorological conditions

The system was first evaluated through simulation under ordinary test scenarios (25°C &1000 W/m²). The simulation was run using the Rao-1 algorithm, which is simulated in the MATLAB/Simulink software. The Rao-1 algorithm, which is implemented in the MATLAB/Simulink environment, was used to run the simulation. The findings demonstrated the system's maximum power output of 75.0779 W. Moreover, the simulated voltage and current profiles closely match the manufacturer's specifications, demonstrating that the developed model accurately replicates the mechanism's electrical behavior under standard test conditions. This agreement confirms the reliability of the simulation for further analysis. Figure 20 presents the corresponding current, voltage, and power characteristic curves, highlighting the system's performance and MPPT under the given operating conditions.

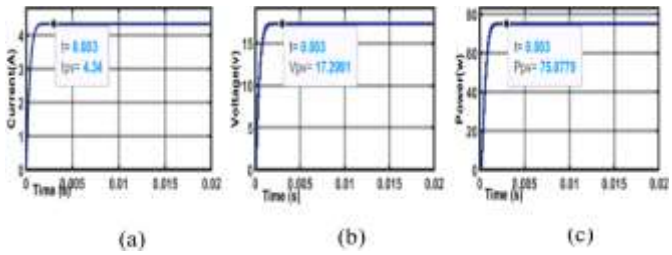

Figure 20. PV characteristic with Maximum Power Point (MPPT) using Rao1 at STC, (a) Current, (b) Voltage, (c) Power

Under conditions identical to the previous tests, the performance of the new Rao 1 controller was further evaluated via MATLAB/Simulink. The Rao1 controller was benchmarked against the metaheuristic PSO algorithm and the classical P&O technique.

The simulation results, visually represented in Figure 21 and detailed quantitatively in Table 3, indicated promising results for the Rao-1 controller.

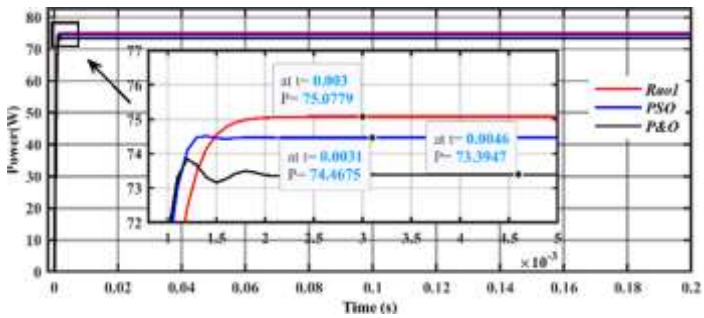

Figure 21. Maximum Power Point (MPPT) tracking using Rao-1, Particle Swarm Optimization (PSO) and Perturb and Observe (P&O) controller at STC

Table 3. Analysis of simulation performance comparison validated against STD

Parameter	Rao-1	PSO	P&O
MPPT	75.0779	74.4675	73.394
Convergence time (ms)	3	3.1	5
Actual Power (w)	75.104	75.104	75.104
Relative error (%)	0.035	0.855	2.329
Efficiency (%)	99.965	99.145	97.671

The graphical and numerical results shown in Figure 21 and Table 3 are used to examine the ability of three approaches to maximize solar power output at STC circumstances. The performance of each of the three methods is described as follows:

Rao-1 is the most accurate and efficient algorithm in this case. It estimates the maximum power at 75.0779 W, very close to the actual 75.1047 W, leading to the lowest relative error (0.035%) and the highest efficiency (99.965%). It also has the fastest response time, reaching convergence in 3.0 ms.

PSO performs slightly worse than Rao-1. Its power estimate is less accurate, with a relative error of 0.855% and an

efficiency of 99.145%. However, its convergence time (3.1 ms) is almost the same as Rao-1.

The third strategy, perturbation and observation, has the worst results, with the largest relative error (2.329%), the lowest efficiency (97.671%), and the slowest convergence time (5 ms).

Overall, Rao-1 is the best-performing MPPT method in this scenario, followed by PSO, while P&O lags behind in both accuracy and speed.

3.2 Dynamic meteorological conditions

The alternation between the appearance and disappearance of the sun, due to intermittent cloud cover, especially in winter, leads to rapid variations in light intensity and temperature. In this dynamic scenario, MATLAB simulations were conducted to compare the performance of the Rao1, PSO, and P&O MPPT algorithms in terms of their ability to maximize energy output.

Initially, from 0 to 0.05 s, the solar irradiance was regulated by1000 W/m² while the temperature by 25°C. At 0.05 s, the irradiance dropped abruptly to 900 W/m² whereas the temperature decreased to 20°C, remaining at these levels until 0.1 s. By 0.1 s, the radiation further reduced to 700 W/m², accompanied by a temperature drop to 15°C. Finally, at 0.15 s, the irradiance returned to 1000 W/m², with the temperature rising back to 25°C. The climatic condition variations during the test period are shown in Figure 22.

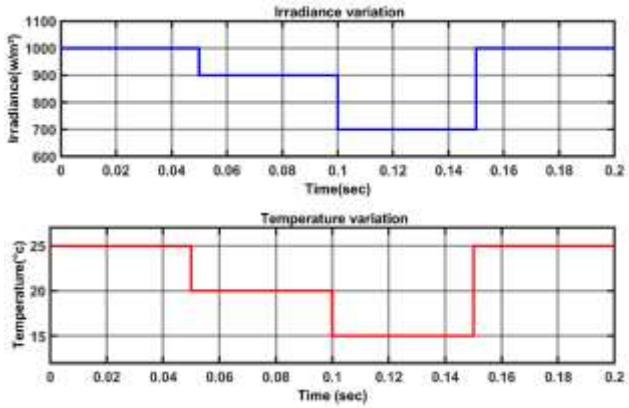

Figure 22. Dynamic meteorological conditions

Figure 23 depicts the effectiveness comparison of Rao1 with PSO and P&O strategies during various test conditions. The achievement is evaluated based on the power generated versus time. By comparing the curves in each case, one can analyse the speed, stability, and efficiency of each algorithm. For example, one can observe whether the new algorithm reaches higher power faster, or whether it exhibits significant.

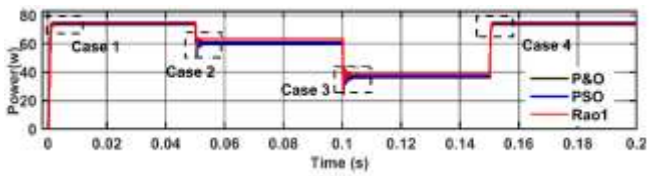

Figure 23. Output power of the three techniques in varying meteorological scenarios

Figure 24 compares the efficiency of three MPPT approaches in the context of maximum power extraction under different insolation levels and temperature degrees. Each subfigure represents a distinct test scenario and illustrates the PV system power–time response. The results highlight significant differences in convergence speed, stability, and steady-state power, while the enlarged views provide clearer insight into the transient convergence behavior of the algorithms.

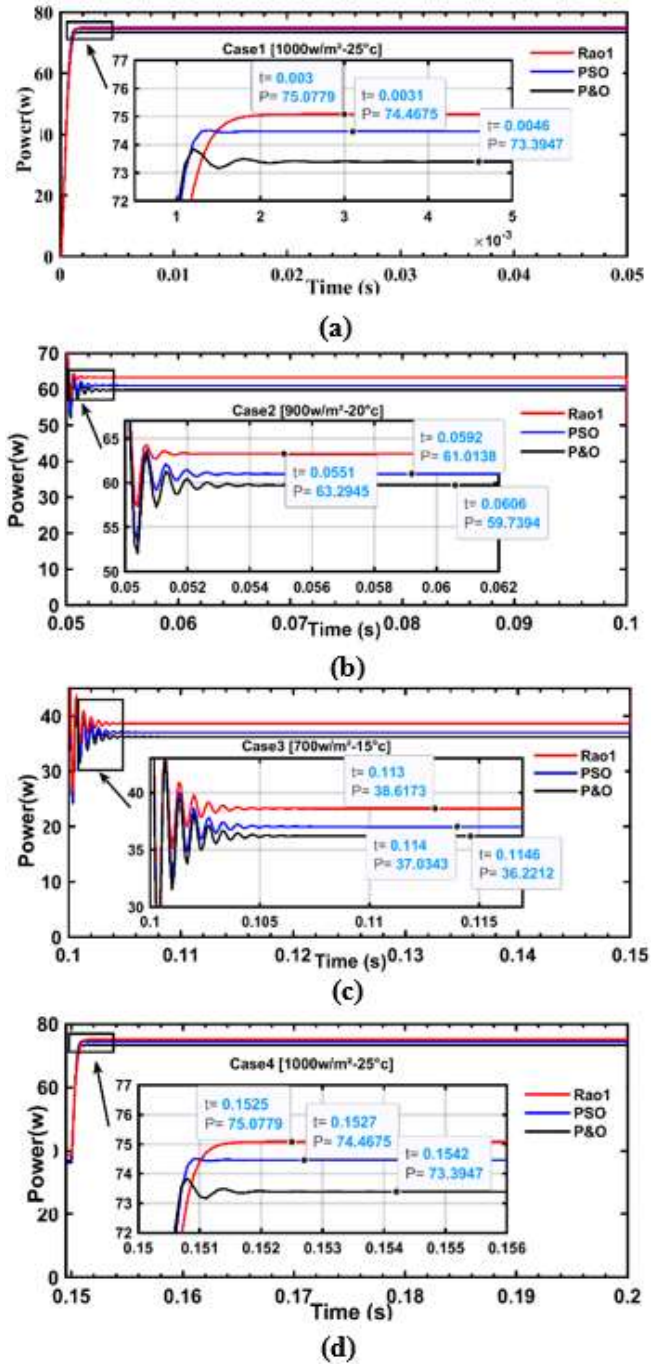

Figure 24. Output power with convergence time of the three algorithms, (a) case1, (b) case2, (c) case3 and (d) case4

In Case 1 (1000 W/m², 25°C), shown in Figure 24(a), Rao1 demonstrates superior dynamic performance, achieving 75.08 W in only 0.003 s with negligible overshoot. PSO follows closely, attaining 74.47 W in 0.0031 s, whereas P&O exhibits slower convergence and oscillatory behavior, stabilizing at 73.39 W in 0.0046 s.

Under Case 2 (900 W/m², −20°C), Figure 24(b) reveals a

shift in dynamics: Rao1 remains the fastest (63.29 W in 0.0051 s) but with noticeable oscillations; PSO converges to 61.01 W after 0.0092 s with persistent fluctuations; P&O trails, reaching 59.73 W.

In Case 3 (700 W/m², −15°C), shown in Figure 24(c), Rao-1 again secures the highest power (38.61 W) though with stronger oscillations, while PSO offers smoother but slightly lower performance at 37.03 W, and P&O continues as the least efficient at 36.22 W.

Finally, Case 4 (1000 W/m², 25°C), Figure 24(d), reaffirms Rao-1's dominance with 75.08 W in 0.0025 s, surpassing PSO (74.47 W) and P&O (73.39 W). The summarized numerical outcomes are presented in Table 4.

Figure 25 compares the maximum power extraction performance of the Rao-1, PSO, and P&O algorithms. The subfigures (a, b, c, d) analyze different scenarios, highlighting the length of the initial oscillations (OL). Rao-1 is distinguished by a faster response time and an absence of oscillations, unlike PSO and P&O, which exhibit damped oscillations.

In case 1 (Figure 25(a)), Rao-1 reaches the steady state without overshoot (OL = 0), while PSO and P&O show small oscillations (OL = 0.0767 W and 0.6897 W respectively).

Case 2 (Figure 25(b)) reveals more pronounced oscillations for PSO and P&O (OL = 10.1261 W and 11.2588 W), while Rao-1 shows a slight overshoot (OL = 6.9505 W). In case 3 (Figure 25(c)), Rao-1, PSO and P&O exhibit significant oscillations of comparable amplitudes (OL = 17.3563 W, 18.5582 W and 19.0504 W, respectively). Case 4 (Figure 25(d)) reproduces similar results to case 1. These numerical findings are detailed through Table 4.

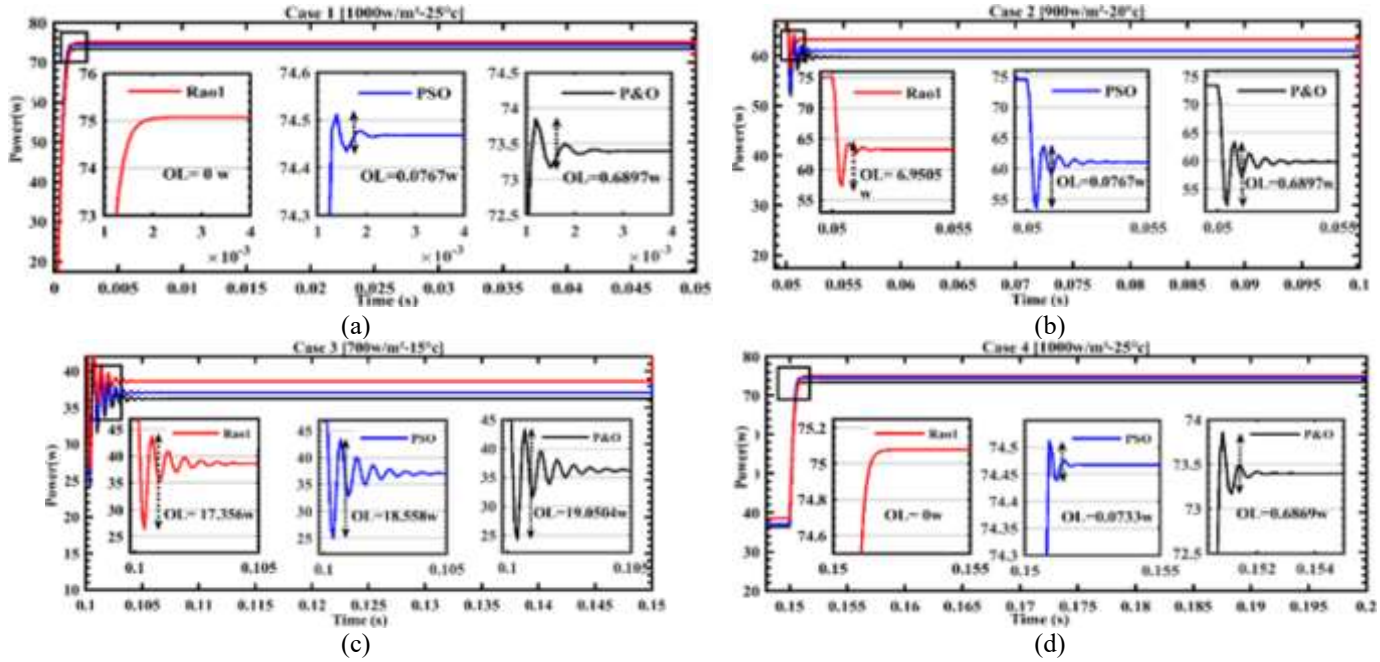

Figure 25. Output power oscillation of three algorithm, (a) case1, (b) case2, (c) case3 and (d) case4

Table 4. Numerical simulation results of Rao-1, Particle Swarm Optimization (PSO), and Perturb and Observe (P&O) methods in variable environmental conditions

	Dynamic meteorological condition		**Case1**	**Case2**	**Case3**	**Case4**
		Irradiation	1000 w/m²	900 w/m²	700 w/m²	1000w/m²
		Temperature	25°C	20°C	15°C	25°C
		time interval (ms)	0 to 50	50 to 100	100 to 150	150 to 200
MPPT Method	**Rao-1**	MPPT (w)	**75.0779**	**63.2945**	**38.6173**	**75.0779**
		Actual MPPT (w)	75.1047	66.3225	41.0052	75.1047
		Efficiency (%)	99.964	95.216	93.816	99.964
		Convergence Time (ms)	3	5.1	13	2.5
		Oscillation length (w)	0	12.4963	14.3067	1.0149
	PSO	MPPT (w)	**74.4675**	**61.0138**	**37.0343**	**74.4675**
		Actual MPPT (w)	75.1047	66.3225	41.0052	75.1047
		Efficiency (%)	99.145	91.3	89.276	99.145
		Convergence Time (ms)	3.1	9.2	14	2.7
		Oscillation length (w)	0.0767	14.1168	14.4647	2.5532
	P&O	MPPT (w)	**73.3947**	**59.7394**	**36.2212**	**73.3947**
		Actual MPPT (w)	75.1047	66.3225	41.0052	75.1047
		Efficiency (%)	97.671	88.981	86.793	97.671
		Convergence Time (ms)	5	10.6	14.6	4.2
		Oscillation length (w)	0.6897	15.7071	13.9033	5.1229

According to the results stated in Table 4, the Rao- metaheuristic consistently outperforms PSO and P&O under

all tested dynamic weather conditions. It achieves higher maximum power efficiency, faster convergence, and reduced steady-state fluctuations, demonstrating clear superiority in better tracking of the MPPT and improved operational stability. All MPPT methods exhibit increased oscillations under medium-to-low irradiance conditions (Cases 2 and 3) due to the flattening of the PV P–V characteristic near the MPPT, which amplifies power fluctuations. However, owing to its population-based search that iteratively moves toward the optimal solution and avoid from the worst, Rao-1 maintains improved stability around the MPPT and exhibits fewer oscillations than PSO and P&O.

4. CONCLUSIONS

This study shows that the Rao-1 algorithm is an effective MPPT control method for solar energy systems utilizing the ISOPHOTON IS-75/12 module. MATLAB/Simulink simulations indicate that Rao-1 operates more efficiently compared to the conventional P&O and PSO methods, exhibiting faster convergence, greater tracking accuracy, and more stable operation under varying insolation and temperature scenarios. Although the current analysis is limited to simulation results and does not include partial shading effects or different load conditions, the findings suggest that Rao-1 is a reliable and computationally efficient MPPT approach. Future work will focus on experimental and Validation through hardware simulation, including FPGA-based implementation, testing under partial shading conditions, and comparison with other advanced metaheuristic algorithms to better evaluate its practical performance.

REFERENCES

[1] Strielkowski, W., Civín, L., Tarkhanova, E., Tvaronavičienė, M., Petrenko, Y. (2021). Renewable energy in the sustainable development of electrical power sector: A review. Energies, 14(24): 8240. https://doi.org/10.3390/en14248240

[2] Chala, G.T., Al Alshaikh, S.M. (2023). Solar photovoltaic energy as a promising enhanced share of clean energy sources in the future. A comprehensive review. Energies, 16(24): 7919. https://doi.org/10.3390/en16247919

[3] Huang, X., Han, S., Huang, W., Liu, X. (2013). Enhancing solar cell efficiency: The search for luminescent materials as spectral converters. Chemical Society Reviews, 42(1): 173-201. https://doi.org/10.1039/C2CS35288E

[4] Green, M., Dunlop, E., Hohl-Ebinger, J., Yoshita, M., Kopidakis, N., Hao, X. (2021). Solar cell efficiency tables (version 57). Progress in Photovoltaics: Research and Applications, 29(1): 3-15. https://doi.org/10.1002/pip.3371

[5] Gohar Ali, H., Vilanova Arbos, R., Herrera, J., Tobón, A., Peláez-Restrepo, J. (2020). Non-linear sliding mode controller for photovoltaic panels with maximum power point tracking. Processes, 8(1): 108. https://doi.org/10.3390/pr8010108

[6] Cakmak, R., Altas, I.H., Sharaf, A.M. (2012). Modeling of FLC-Incremental based MPPT using DC-DC boost converter for standalone PV system. In 2012 International Symposium on Innovations in Intelligent Systems and Applications, Trabzon, Turkey, pp. 1-5. https://doi.org/10.1109/INISTA.2012.6246932

[7] Yu, X., Wu, X., Luo, W. (2022). Parameter identification of photovoltaic models by hybrid adaptive JAYA algorithm. Mathematics, 10(2): 183. https://doi.org/10.3390/math10020183

[8] Hussien, A.G., Bouaouda, A., Alzaqebah, A., Kumar, S., Hu, G., Jia, H. (2024). An in-depth survey of the artificial gorilla troops optimizer: Outcomes, variations, and applications. Artificial Intelligence Review, 57(9): 246. https://doi.org/10.1007/s10462-024-10838-8

[9] Kana, A., Ahmad, I. (2023). An effective Runge-Kutta optimizer based on adaptive population size and search step size. Computers, Materials & Continua, 76(3): 3443-3464. https://doi.org/10.32604/cmc.2023.040775

[10] Rao, R.V. (2020). Rao algorithms: Three metaphor-less simple algorithms for solving optimization problems. International Journal of Industrial Engineering Computations, 11(1): 107-130. https://doi.org/10.5267/j.ijiec.2019.6.002

[11] Sharma, A.K., Pachauri, R.K., Choudhury, S., Minai, A.F., Alotaibi, M.A., Malik, H., Márquez, F.P.G. (2023). Role of metaheuristic approaches for implementation of integrated MPPT-PV systems: A comprehensive study. Mathematics, 11(2): 269. https://doi.org/10.3390/math11020269

[12] Patel, G., Patel, D.B., Paghdal, K.M. (2016). Analysis of P&O MPPT algorithm for PV system. International Journal of Electrical and Electronics Engineering, 5(6): 1-10. https://www.academia.edu/download/50672767/1._IJEEE_-__Analysis_of_PO_MPPT_Algorithm_for_PV_System.pdf.

[13] Hasan, M.A., Parida, S.K. (2016). An overview of solar photovoltaic panel modeling based on analytical and experimental viewpoint. Renewable and Sustainable Energy Reviews, 60: 75-83. https://doi.org/10.1016/j.rser.2016.01.087

[14] Al-Ezzi, A.S., Ansari, M.N.M. (2022). Photovoltaic solar cells: A review. Applied System Innovation, 5(4): 67. https://doi.org/10.3390/asi5040067

[15] Devasia, A., Kurinec, S.K. (2011). Teaching solar cell IV characteristics using SPICE. American Journal of Physics, 79(12): 1232-1239. https://doi.org/10.1119/1.3636525

[16] Nguyen-Duc, T., Nguyen-Duc, H., Le-Viet, T., Takano, H. (2020). Single-diode models of PV modules: A comparison of conventional approaches and proposal of a novel model. Energies, 13(6): 1296. https://doi.org/10.1119/1.3636525

[17] Tian, H., Mancilla-David, F., Ellis, K., Muljadi, E., Jenkins, P. (2012). Detailed performance model for photovoltaic systems (No. NREL/JA-5500-54601). National Renewable Energy Lab. (NREL): Golden, CO (United States).

[18] Raya-Armenta, J.M., Ortega, P.R., Bazmohammadi, N., Spataru, S.V., Vasquez, J.C., Guerrero, J.M. (2021). An accurate physical model for PV modules with improved approximations of series-shunt resistances. IEEE Journal of Photovoltaics, 11(3): 699-707 https://doi.org/10.1109/JPHOTOV.2021.3056668

[19] Tsai, H.L., Tu, C.S., Su, Y.J. (2008). Development of

generalized photovoltaic model using MATLAB/Simulink. Proceedings of the World Congress on Engineering and Computer Science, San Francisco, US, 200: 1-6. https://www.iaeng.org/publication/WCECS2008/WCECS2008_pp846-851.pdf.
[20] Verma, D., Nema, S., Agrawal, R., Sawle, Y., Kumar, A. (2022). A different approach for maximum power point tracking (MPPT) using impedance matching through non-isolated DC-DC converters in solar photovoltaic systems. Electronics, 11(7): 1053. https://doi.org/10.3390/electronics11071053
[21] Nasiri, M., Chandra, S., Taherkhani, M., McCormack, S.J. (2021). Impact of input capacitors in boost converters on stability and maximum power point tracking in PV systems. In 2021 IEEE 48th Photovoltaic Specialists Conference (PVSC), pp. 1004-1008. https://doi.org/10.1109/PVSC43889.2021.9518903
[22] Bhatnagar, P., Nema, R.K. (2013). Maximum power point tracking control techniques: State-of-the-art in photovoltaic applications. Renewable and Sustainable Energy Reviews, 23: 224-241. https://doi.org/10.1016/j.rser.2013.02.011
[23] Killi, M., Samanta, S. (2015). Modified perturb and observe MPPT algorithm for drift avoidance in photovoltaic systems. IEEE Transactions on Industrial Electronics, 62(9): 5549-5559. https://doi.org/10.1109/TIE.2015.2407854
[24] Katche, M.L., Makokha, A.B., Zachary, S.O., Adaramola, M.S. (2023). A comprehensive review of maximum power point tracking (MPPT) techniques used in solar PV systems. Energies, 16(5): 2206. https://doi.org/10.3390/en16052206
[25] Mahmod Mohammad, A.N., Mohd Radzi, M.A., Azis, N., Shafie, S., Atiqi Mohd Zainuri, M.A. (2020). An enhanced adaptive perturb and observe technique for efficient maximum power point tracking under partial shading conditions. Applied Sciences, 10(11): 3912. https://doi.org/10.3390/app10113912
[26] Eberhart, R., Kennedy, J. (1995). A new optimizer using particle swarm theory. In MHS'95. Proceedings of the Sixth International Symposium on Micro Machine and Human Science, pp. 39-43. https://doi.org/10.1109/MHS.1995.494215
[27] Abdulkadir, M., Yatim, A.H.M., Yusuf, S.T. (2014). An improved PSO-based MPPT control strategy for photovoltaic systems. International Journal of Photoenergy, 2014(1): 818232. https://doi.org/10.1155/2014/818232
[28] Elsheikh, A.H., Abd Elaziz, M. (2019). Review on applications of particle swarm optimization in solar energy systems. International Journal of Environmental Science and Technology, 16(2): 1159-1170. https://doi.org/10.1007/s13762-018-1970-x
[29] Rezk, H., Fathy, A., Abdelaziz, A.Y. (2017). A comparison of different global MPPT techniques based on meta-heuristic algorithms for photovoltaic system subjected to partial shading conditions. Renewable and Sustainable Energy Reviews, 74: 377-386. https://doi.org/10.1016/j.rser.2017.02.051
[30] Hayder, W., Ogliari, E., Dolara, A., Abid, A., Ben Hamed, M., Sbita, L. (2020). Improved PSO: A comparative study in MPPT algorithm for PV system control under partial shading conditions. Energies, 13(8): 2035. https://doi.org/10.3390/en13082035
[31] A. Alturki, F., Al-Shamma'a, A.A., MH Farh, H. (2020). Simulations and dSPACE real-time implementation of photovoltaic global maximum power extraction under partial shading. Sustainability, 12(9): 3652. https://doi.org/10.3390/su12093652
[32] Ku, J., Li, S., Gong, W. (2022). Photovoltaic models parameter estimation via an enhanced Rao-1 algorithm. Mathematical Biosciences and Engineering, 19: 1128-1153. https://doi.org/10.3934/mbe.2022052

NOMENCLATURE

DC-DC	Direct Current to Direct Current
DC-AC	Direct Current to Alternating Current
OL	Oscillation length
F	Farad
H	Henry
Hz	Hertz
Ω	Ohm